Received: 11 November 2020 | Revised: 7 January 2021 | Accepted: 7 January 2021

DOI: 10.1111/jace.17690

Journal of the American Ceramic Society

ORIGINAL ARTICLE

Photoelastic confirmation of surface stress relaxation in silica glasses: Fiber bending and rod torsion

Bronson D. Hausmann | **Emily M. Aaldenberg** | **Minoru Tomozawa**

Department of Materials Science and Engineering, Rensselaer Polytechnic Institute, Troy, NY, USA

Correspondence
Minoru Tomozawa, Department of Materials Science and Engineering, Rensselaer Polytechnic Institute, Troy, NY 12180, USA.
Email: tomozm@rpi.edu

Present address
Emily M. Aaldenberg, Corning Incorporated, Painted Post, NY 14870, USA

Funding information
Division of Materials Research, Grant/Award Number: DMR-1713670; Corning Incorporated

Abstract

Silica glass samples were given various heat treatments under stress at low temperatures and subsequently their residual stress distributions in terms of retardance were observed using a polarized light microscope, confirming previously reported fast surface stress relaxation while providing more detailed characterization. Retardance profiles of silica glass fibers heat-treated under a constant bending strain in the presence of atmospheric water vapor were measured and fit to a previously developed diffusion-based relaxation model. The retardance of a cross-section of a silica glass rod heat-treated at 650°C in lab air under applied torsional shear strain was also measured to confirm the presence of residual surface shear stress which was predicted by the decrease of torque with time for the rod. Together, these results confirm the low-temperature fast surface stress relaxation which occurs when water vapor is present for both bending and shear stresses.

KEYWORDS

birefringence, diffusion/diffusivity, silica, stress relaxation

1 | INTRODUCTION

Fast surface stress relaxation in silica glass has been found to occur at low temperatures in the presence of water vapor.[1] Various methods have been employed to characterize surface stress relaxation in glass fibers including IR spectroscopy,[2] fiber bending relaxation kinetics,[3] and fiber strengthening by surface stress relaxation.[1,4] Surface stress relaxation has been used to account for phenomena such as crack toughening by tensile stress application below the fatigue limit, region zero in the slow crack growth velocity vs stress intensity diagram,[5,6] and the corresponding static fatigue limit of glass.[6,7] Shear stress relaxation of silica rods at low temperatures has been similarly attributed to interaction with ambient water vapor.[8]

Previous calculations of the surface stress relaxation rate or residual stress in the glass surface were made from various measurable quantities of stress relaxation, such as the failure strength in bending, fiber bending residual curvature, or torque relaxation under applied shear strain.[3,8,9] In all configurations, it was assumed that the relaxation advances from the sample surface in a diffusion-controlled manner with the relaxation depth given by

$$z = \sqrt{D_{SSR} \cdot t} \tag{1}$$

where z is the depth of 50% surface relaxation, such that full relaxation occurs at $2z$, D_{SSR} is the effective diffusivity of surface stress relaxation, and t is the time duration of heat treatment. Discussion of the stress relaxation rate as an effective diffusivity limited by water diffusion allows for analysis of the process kinetics, which are different from the water diffusion itself. In this paper, residual stresses near the glass surface of both silica glass fibers and rods were measured through optical retardation and compared with the theoretical stress produced by fast surface stress relaxation after the samples were heat-treated at a temperature far below the glass transition temperature in lab air while under applied strain.

Optical measurements were made using a polarized light microscope (Nikon Eclipse, LV-100 NPOL) using the Senarmont method, which has been used to measure stress profiles in optical fibers previously.[10-12] The intensity of cross-polarized light passing through the sample and a quarter wave plate was analyzed in order to produce retardance profiles across the field of view of the microscope. Retardance can be related to the stress, σ in glass by the stress optic law:[13]

$$\sigma = \frac{\Delta}{C \cdot y} \tag{2}$$

where Δ is the retardance, C is the stress optic coefficient, and y is the path length through the material.

2 | FIBER BENDING

2.1 | Analysis of residual bending stress

Previously, surface stress relaxation kinetics were measured based on the residual curvature of fiber heat-treated in a two-point bend configuration. A simplified analysis related the difference in angle between the straight portion of the fiber tail (where no bend was applied) and the original straight fiber, Φ in radians, to the radius of curvature of the fiber[3]

$$\Phi = \frac{R_0}{R_S} \cdot \frac{\pi}{2} \tag{3}$$

where R_0 is the radius of curvature of the fiber during the bending stress application and R_S is the radius of curvature following heat treatment when the fiber is removed from the two-point bending configuration. R_0 and R_S vary as a function of position along the bend, but the ratio R_0/R_S is shown theoretically to be constant at all positions along the curved portion of the fiber. A simple method for obtaining Φ has been developed previously.[14] First, a straight fiber is placed horizontally and a bent fiber is placed, underneath the straight fiber symmetrically. The angle between the horizontal line and straight edge of the bent fiber is given by Φ. Since the residual curvature results from stress distribution in the fiber, photoelastic analysis can be used to determine the curvature from the stress distribution.

The fiber axial stress as a function of radial position is known to be given by the following expression for a known bending radius R_0:

$$\sigma_{\text{applied}}(r,\theta) = \frac{E \cdot r \cdot \cos\theta}{R_0} \tag{4}$$

where E is the Young's modulus and r and θ are the polar coordinates within the fiber (see Figure 1). As fibers under applied stress are heated and undergo surface stress relaxation,

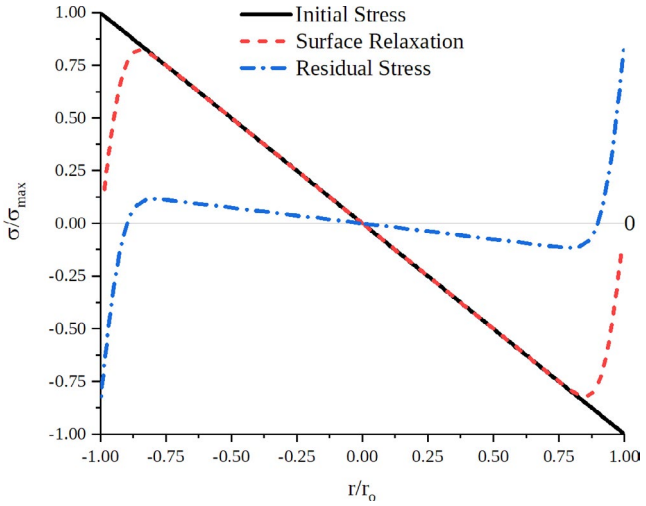

FIGURE 1 Schematic stress profile of surface stress relaxation in bending.[14] A bending moment is applied resulting in an initial stress profile (Equation 4). Upon heat treatment in the presence of water, surface stress relaxation takes place (Equation 5). Here, relaxation is assumed to follow an complementary error function with all stress relaxed at $x = r_o$. After removing the applied bending, the residual stress in the near-surface which was previously under compression is now in tension and vice versa (Equation 8 and Equation 11). The interior stress, however, retains the same sign as the initial stress. The relaxation depth $z/r_o = 0.05$ is over-exaggerated for visibility [Color figure can be viewed at wileyonlinelibrary.com]

the degree of relaxation from the surface inward, $\Delta\sigma_{\text{relax}}$, is assumed to follow a complimentary error function:

$$\Delta\sigma_{\text{relax}}(r,\theta) = \frac{E \cdot r \cdot \cos\theta}{R_0} \cdot erfc\left(\frac{r_0 - r}{2z}\right) \tag{5}$$

where r_0 is the fiber radius. The residual stress is then related to the applied stress and the relaxation ($\Delta\sigma_{\text{relax}}$) with an additional contribution from the elastic response of the fiber upon removal of applied bending ($\Delta\sigma_{\text{spring}}$):

$$\begin{aligned}\sigma_{\text{res}}(r,\theta) &= \frac{E \cdot r \cdot \cos\theta}{R_0} - \Delta\sigma_{\text{relax}} - \Delta\sigma_{\text{spring}} \\ &= \frac{E \cdot r \cdot \cos\theta}{R_S} - \Delta\sigma_{\text{relax}}\end{aligned} \tag{6}$$

where $\Delta\sigma_{\text{spring}} = E \cdot r \cdot \cos\theta \left(\frac{1}{R_0} - \frac{1}{R_s}\right)$.[1] Combining Equation 5 and Equation 6, the residual stress can be expressed as follows:

$$\sigma_{res}(r,\theta) = E \cdot \left\{ \frac{r \cdot cos\theta}{R_S} - \frac{r \cdot cos\theta}{R_0} \cdot erfc\left(\frac{r_0 - r}{2z}\right) \right\} \tag{7}$$

The cross-section of a silica fiber with radius r_0 is schematically shown in Figure 1, demonstrating this theoretical residual stress following heat treatment under bending stress. In rectangular coordinates, this can be rewritten as

$$\sigma_{res}(x,y) = E \cdot \left\{ \frac{x}{R_S} - \frac{x}{R_0} \cdot erfc\left(\frac{r_0 - \sqrt{x^2+y^2}}{2z} \right) \right\} \quad (8)$$

which allows for the coordinates of the theory to align with the measured data, where fiber radial position x is parallel to the stage, as shown in Figure 1.

Experimentally, the fiber geometry and the applied bending curvature are known. Thus, as currently written, Equation 8 requires the measurement of the residual curvature R_S and relaxation depth z to give the residual stress as a function of x position. The residual curvature however is necessarily dependent on the experimental conditions and relaxation depth, because the bending moment of the fiber must be equal to zero under zero applied bending strain[1]:

$$M = 0 = \int_0^{2\pi} \int_0^{r_0} \left\{ E\frac{r}{R_s}cos\theta - E\frac{r}{R_0}cos\theta \cdot erfc\left[\frac{r_0 - r}{2z}\right] \right\} \cdot r^2 cos\theta \; dr \; d\theta \quad (9)$$

where M is the bending moment of the fiber. This integral has been evaluated for the case when $z \ll r_0$ to give the simplified form[1]:

$$M = 0 = \pi E \left[\frac{r_0^4}{4R_S} - \frac{1}{R_0}\left(\frac{2}{\sqrt{\pi}} r_0^3 z \right) \right]$$

$$\frac{r_0}{4R_s} = \frac{2z}{\sqrt{\pi} R_0}$$

thus

$$R_s = \frac{\sqrt{\pi} R_0 r_0}{8\, z} \approx \frac{R_0 r_0}{4.51\, z} \quad (10)$$

Equation 8 can therefore be rewritten in terms of z, r_0, and R_0 alone, eliminating R_s by substitution with Equation 10:

$$\sigma_{res}(x,y) = E \cdot \left\{ \frac{4.51 \cdot z \cdot x}{R_0 \cdot r_0} - \frac{x}{R_0} \cdot erfc\left(\frac{r_0 - \sqrt{x^2+y^2}}{2z} \right) \right\} \quad (11)$$

A residual stress profile can thus be fit to find the parameter z for $z << r_o$ since the applied radius of curvature R_0 and the fiber radius r_0 are known. Figure 2 shows the initial stress distribution in the fiber along y = 0 (the case when the fiber is in focus on the microscope) when the bending moment is applied, the stress after relaxation has occurred to a depth z, and the residual stress following heat treatment and removal from the initial bend.

2.2 | Experimental procedure

Suprasil II silica fibers (Heraeus Inc.) were characterized following fiber bending relaxation. The fiber contains 1200 wt. ppm OH and 0.1 wt. ppm Al, with all other impurities less than 0.05 wt. ppm. The Young's modulus of the fiber is 72.0 GPa and the stress optic coefficient is 3.19 Brewsters.[15] The glass transition temperature was estimated to be ~952°C-1006°C.[16,17] Fibers with a diameter, $2r_0$, of 125 μm were placed in a static two-point bending configuration using 15, 20, and 22 mm inner diameter silica glass tubes. This configuration gave an initial maximum bending stress of 728, 545, and 495 MPa, respectively, at the apex of the bend.[9] Fibers were then heat-treated in lab air at 300-500°C for various lengths of time, up to 17 days. The partial pressure of water in the lab air was estimated to be about 7 Torr, or 1 kPa, as assumed in previous fiber bending experiments. Following relaxation, the fibers that were removed from the tubes exhibited a residual bend from the surface stress relaxation during heat treatment.

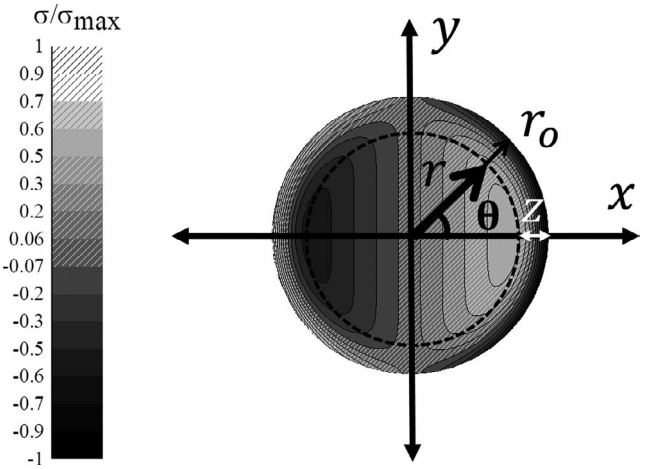

FIGURE 2 Schematic of the residual stress distribution in a fiber cross-section with radius r_o following removal of the applied bend after relaxation in a two-point bending configuration. The relaxation depth is denoted by z. At the apex of the bend, the maximum tensile strain was applied at position ($x = r_o$, $y = 0$) during bending and the maximum compressive strain was applied at position ($x = -r_o$, $y = 0$). This results in a residual stress in the fiber axial direction of opposite sign of the applied strain, compressive stress at ($x = r_o$, $y = 0$) and tensile at ($x = -r_o$, $y = 0$) for example. Polarized light was passed through the sample in the y direction in order to measure the stress distribution in the fiber as a function of x

Stress birefringence measurement of silica glass fibers was described in detail in previous work.[18] In this experiment also, fibers were placed upon slides in index-matching fluids and the retardance integrated along the x direction of the entire fiber cross-section shown in Figure 1 was determined. Polarized light was passed through the sample along the y-axis in order to measure this retardance in order to calculate the residual stress in the fiber axial direction. Following bending relaxation and subsequent removal from this configuration, the residual stress distribution is expected to follow Equation 11.

This theoretical stress distribution can be converted to retardance as a function of position x by application of Equation 2:[18]

$$\Delta(x) = \int_{y_{min}=-\sqrt{r_o^2-x^2}}^{y_{max}=\sqrt{r_o^2-x^2}} C \cdot \{\sigma_{res}(x,y)\}\, dy \qquad (12)$$

where y_{min} and y_{max} determine the sample thickness at position x. To avoid including the residual stress present from the fiber drawing process in this analysis, the retardance profile of an as-received fiber was subtracted from the retardance measured following relaxation. Retardance profiles presented in this work are given with negative retardance plotted in the positive y direction, in order to match previous work.[18] Retardance was fit to Equation 11 and Equation 12 using only z as the fitting parameter, as C, E, R_0, and r_o are known. The z parameter was substituted into Equation 1 and fit as a function of heat treatment time in order to calculate effective diffusivity of surface stress relaxation. For comparison, Φ was also measured. Substitution of Equation 10 into Equation 3 gives Φ in terms of z, which allows for direct comparison.[1]

$$\Phi = \frac{R_0}{R_S} \cdot \frac{\pi}{2} = \frac{4.51\pi z}{2r_0} \qquad (13)$$

2.3 | Results

Bending relaxation of silica glass fibers resulted in the expected stress distribution predicted by Lezzi et al[3] when retardance of the as-received fiber is removed (see Figure 3).[18] Several retardance profiles were fit to Equation 12. Examples of the fit are shown in Figure 4 and Figure 5.

The diffusivity of surface stress relaxation has been calculated through a linear fit of z^2 as a function of t at a given temperature. These diffusivities were organized into an Arrhenius plot as shown in Figure 6, which were found to follow to a single line with an activation energy of 122 ± 8 kJ/mol.

Diffusivity was also calculated using the fiber bending angle and compared to the values obtained by retardance measurement in this work, as well as previously obtained values[19] from bending angle measurements (see Figure 7). New calculations of diffusivity by bending angle resulted in an activation energy calculation of 109 ± 14 kJ/mol. The diffusivity values calculated using the retardance method were consistently lower than those calculated using the bending angle measurement method for the same samples (see Table 1).

Figure 8 compares the surface stress relaxation diffusion coefficients determined using the two different methods. The two methods give diffusivity within 10 percent of each other, although fiber bending angle measurement consistently resulted in a higher diffusivity calculation.

2.4 | Discussion

Diffusivity values measured via birefringence are consistent with the fiber bending angle measurement method developed previously within the measurable temperature range, affirming previous predictions above 300°C.[1] Diffusivity of surface stress relaxation for silica glass with various impurities was measured previously in the temperature range 400-700°C. Within this temperature range, a single activation energy, higher than observed in this work, was observed of ~164-188 kJ/mol.[1,19] The difference in measured diffusivity of bending angle and retardance may be a result of changes in the fiber surface stress optic coefficient or elastic modulus via increased water content following heat treatment.

The diffusivity of surface stress relaxation appears to be slightly higher for surfaces under compression (see Figure 5). This result has also been shown previously for water diffusion in

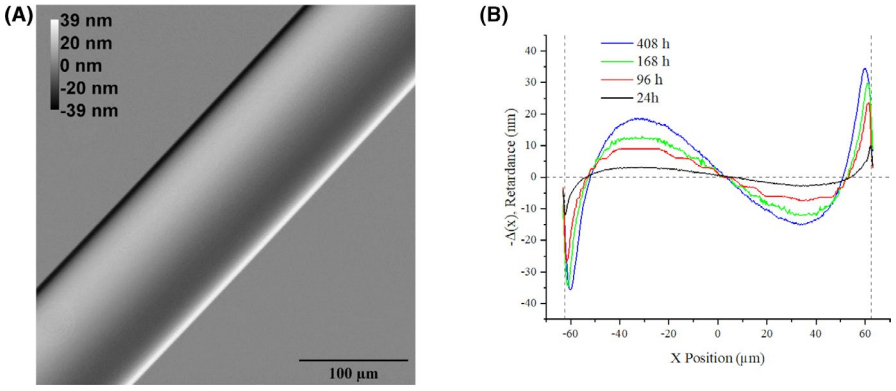

FIGURE 3 (A) Example of a measured fiber bending retardance map of a 500°C, 408 h treatment as measured with retardance profile. The positive y direction corresponds to negative retardance and thus residual compressive stress. (B) Theory fit following heat treatments at 500°C from 24 to 408 h under a maximum bending stress of 728 MPa. Fiber edges are indicated by vertical lines [Color figure can be viewed at wileyonlinelibrary.com]

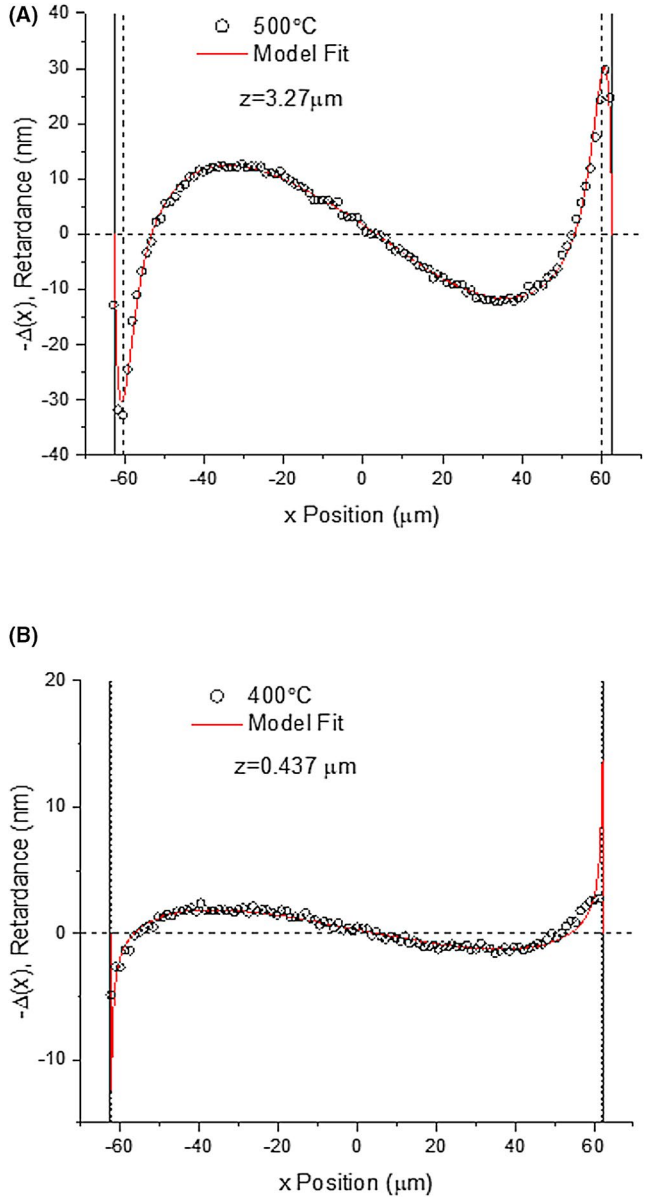

FIGURE 4 Fiber bending retardance data fit using Equation 12. Curves are shown to fit to the optical retardance measurements for samples heat-treated at (A) 500°C and (B) 400°C with a maximum bending stress of 728 MPa for 168 hours. In this case, the tensile and compressive stress fits of depth z do not appear to differ significantly. The fiber surface is indicated by solid vertical lines, with z depth indicated by dashed lines. Retardance corresponding to compressive stress is positive [Color figure can be viewed at wileyonlinelibrary.com]

thin glass plates under bending, in which the stress dependence of water diffusivity changes trend in the same manner seen here in bending stress relaxation diffusivity.[20] Previous work has also found that OH diffusivity is time dependent at low temperatures due to the non-equilibrium nature of its reaction with the silica network.[21] As the stress relaxation diffusivity is dependent on diffusion of water, it is possible that at low temperatures the relaxation diffusivity may also be time dependent. This may be investigated with longer time relaxation experiments or by altering environmental water concentration.

The presence of a small residual stress in the as-received fiber may have also influenced the diffusivity of surface stress relaxation. The fiber used in this work was found to have a small residual compressive stress at the surface prior to heat treatment, which may have resulted in an underestimation of applied compressive stress as well as an

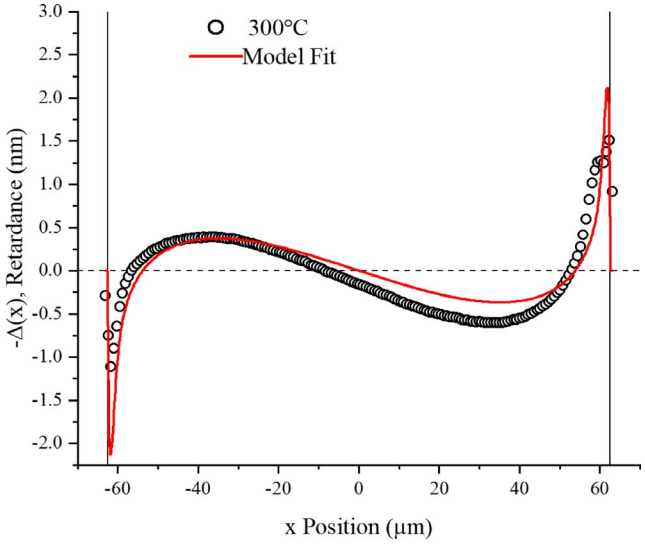

FIGURE 5 Fiber bending retardance profile for sample heat-treated at 300°C under a maximum bending stress of 728 MPa for 168 hours. The slight deviation between peak widths for the side which was heated under compression (left) versus tension (right) is apparent at this lower temperature [Color figure can be viewed at wileyonlinelibrary.com]

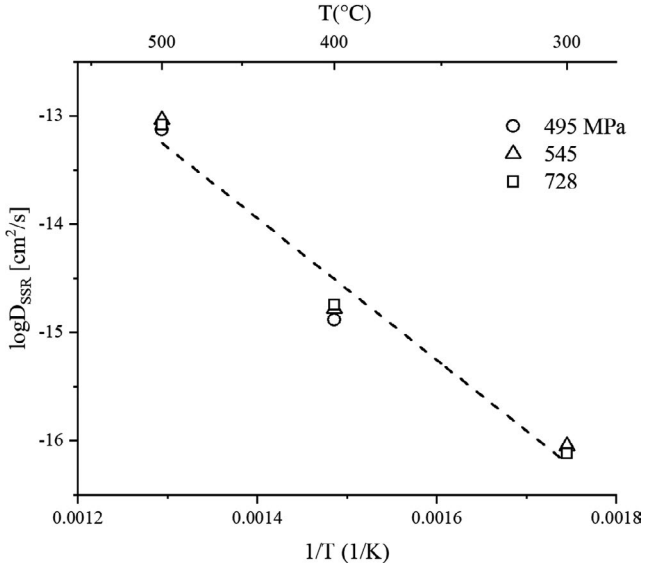

FIGURE 6 Arrhenius plot of bending relaxation diffusivity for various stress values. The line indicates activation energy of 122 ± 8 kJ/mol

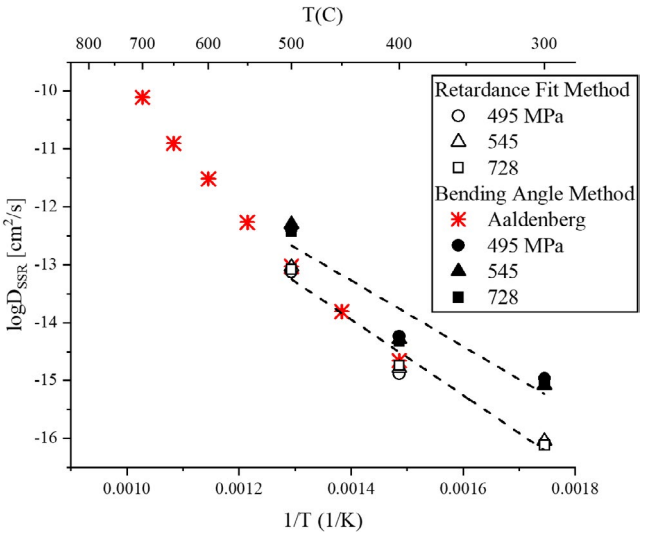

FIGURE 7 Arrhenius plot comparing diffusivity measurement methods as applied in this work and previous work.[19] This work's measurements are differentiated by applied stress. Dashed lines indicate the activation energy fit for retardance and bending angle diffusivity calculations (122 ± 8 and 109 ± 14 kJ/mol, respectively). In all cases, diffusivity calculated by bending angle measurement was slightly higher than the corresponding retardance measurement calculation [Color figure can be viewed at wileyonlinelibrary.com]

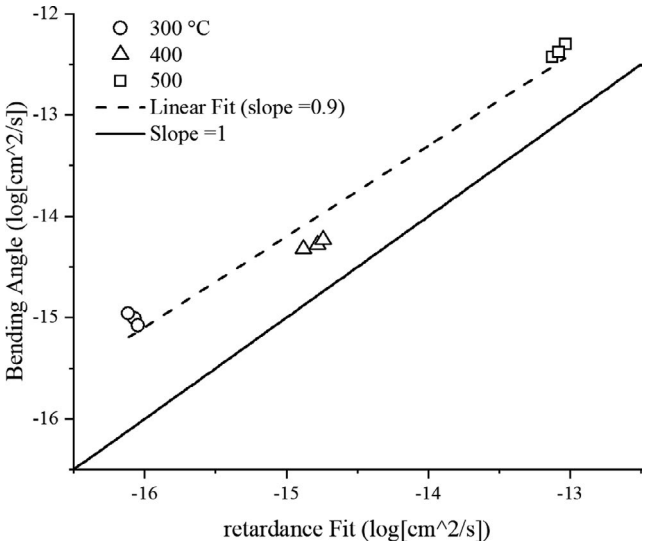

FIGURE 8 Comparison of diffusivity values calculated using the two discussed methods. A linear regression was applied to demonstrate the systematic difference in calculated diffusivities of about 10 percent overall

overestimation of the applied tensile stress at the bending apex. Fiber annealing has been shown to eliminate any measurable retardance caused by residual stress or anisotropy in the as-received fibers.[18] Although annealed fibers have shown some difference in the diffusivity of surface stress relaxation due to changes in fictive temperature, no difference in the activation energy with fictive temperature was observed in the 450-700°C temperature range, previously characterized in silica glass fibers with 1000 ppm Cl impurities.[22] Use of annealed fibers to measure the diffusivity of surface stress relaxation at low temperatures, therefore, would eliminate the effects of residual stress from fiber drawing or anisotropy and additionally remove the need for background subtraction of residual stress.

3 | SHEAR STRESS RELAXATION AND RESIDUAL STRESS

3.1 | Analysis of residual shear stress

Shear strain was applied to a silica glass rod by applying a constant angle of twist. A monotonic decrease in the total torque in the sample was monitored as the rod was heat-treated, demonstrating a stress relaxation over time.[8] At the beginning of the experiment, applied shear stress is a function of radial position

$$\tau_{applied} = \frac{G \cdot r \cdot q}{L} \tag{14}$$

where q is the angle of twist in radians, L is the gage length of the sample, G is the shear modulus, and r is a radial coordinate defined within the rod from $0 \le r \le r_o$. The maximum shear stress, τ_{max}, occurs at $r = r_o$ at time $t = 0$ prior to any relaxation.

Temperature [°C]	Applied Stress [MPa]	D_{SSR}, Retardance [cm^2/s]	D_{SSR}, Bending Angle [cm^2/s]
300	±495	7.67×10^{-17}	9.85×10^{-16}
	±545	8.97×10^{-17}	8.34×10^{-16}
	±728	8.49×10^{-17}	1.10×10^{-15}
400	±495	1.81×10^{-15}	4.78×10^{-15}
	±545	1.66×10^{-15}	5.25×10^{-15}
	±728	1.32×10^{-15}	5.85×10^{-15}
500	±495	8.29×10^{-14}	3.74×10^{-13}
	±545	9.24×10^{-14}	5.01×10^{-13}
	±728	7.48×10^{-14}	4.17×10^{-13}

TABLE 1 Diffusivity of bending stress relaxation, measured by bending angle Φ and retardance fit of z

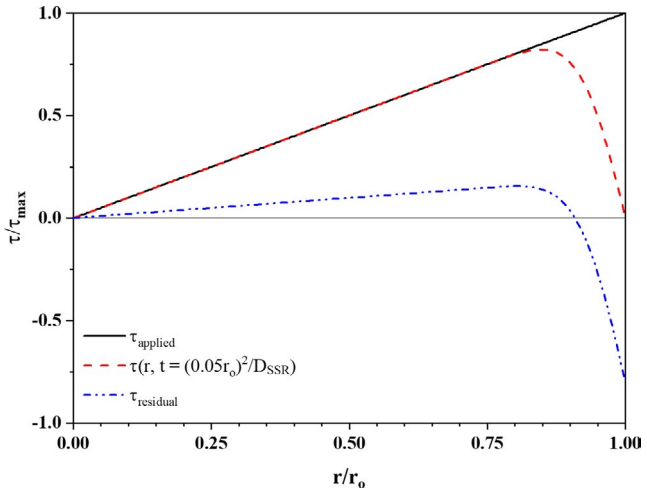

FIGURE 9 Schematic of shear stress relaxation relative to the maximum applied shear stress. Applied stress is defined by Equation 14. Once the stress has relaxed to depth $z = 0.05r_o$, the stress is defined by Equation 16. The residual stress following removal of the applied shear strain is defined by Equation 24 [Color figure can be viewed at wileyonlinelibrary.com]

Similar to the relaxation that occurs in fiber bending, the stress is assumed to relax in a diffusion-controlled manner approximated by the complementary error function. The change in the shear stress due to relaxation is given by Equation 15.

$$\Delta\tau_{relax} = \tau_{applied} \cdot erfc\left(\frac{(r_0 - r)}{2z}\right) \tag{15}$$

The shear stress as a function of radial position and time during the relaxation experiment is therefore defined as

$$\tau(r,t) = \tau_{\text{applied}} - \Delta\tau_{\text{relax}} = \tau_{\text{applied}} \cdot erf\left(\frac{r_0 - r}{2z}\right) \tag{16}$$

The total torque in the sample is a function of time throughout the duration of the heat treatment.

$$T(t) = \int_A \tau(r,t)\, rdA = \int_0^{2\pi}\int_0^{r_0} \tau(r,t)\, r^2 dr\, d\theta \tag{17}$$

where $dA = rdrd\theta$. Substitution of Equation 16 into Equation 17 gives

$$T(t) = G\frac{q}{L}\frac{\pi}{2}\left[\frac{2r_o z\left(-4\left(r_o^2+4z^2\right)+e^{\frac{-r_o^2}{4z^2}}\left(r_o^2+10z^2\right)\right)}{\sqrt{\pi}} + \left(r_o^4+12r_o^2z^2+12z^4\right) erf\left(\frac{r_o}{2z}\right)\right] \tag{18}$$

When $z << r_o$,

$$T(t) = G\frac{q}{L}\frac{\pi}{2}\left[-\frac{8r_o^3 z}{\sqrt{\pi}} + r_o^4 erf\left(\frac{r_o}{2z}\right)\right] \tag{19}$$

At the completion of the rod heat treatment, the applied strain is removed. The rod springs back to an angle of twist per unit length $\frac{q_{\text{spring}}}{L}$, where $\frac{q_{\text{spring}}}{L} < \frac{q}{L}$.

$$\Delta\tau_{\text{spring}} = Gr\left(\frac{q}{L} - \frac{q_{\text{spring}}}{L}\right) \tag{20}$$

The residual shear stress in the rod is defined by

$$\tau_{\text{residual}} = \tau_{\text{applied}} - \Delta\tau_{\text{relax}} - \Delta\tau_{\text{spring}} \tag{21}$$

Since no torque is being applied, the total torque in the rod would become zero.

$$T = 0 = \int_A \tau_{\text{residual}} rdA = \int_0^{2\pi}\int_0^{r_0} \tau_{\text{residual}} r^2 drd\theta \tag{22}$$

Substitution for $\tau_{residual}$ in Equation 22 and solving for $\frac{q_{\text{spring}}}{L}$ gives

$$\frac{q_{\text{spring}}}{L} = \frac{4}{r_o^4}\frac{q}{L}\int_0^{r_0} r^3 erfc\left(\frac{r_o - r}{2z}\right) dr \tag{23}$$

Equation 21 becomes

$$\tau_{\text{residual}} = G\cdot r\cdot\frac{q}{L}\cdot\left[\frac{4}{r_o^4}\int_0^{r_0} r^3\cdot erfc\left(\frac{r_o - r}{2z}\right) dr - erfc\left(\frac{(r_0 - r)}{2z}\right)\right] \tag{24}$$

where z is the only unknown and all other variables are measurable.

A schematic of the shear stress applied to the rod, shear stress after relaxation has occurred to $z = 0.05r_o$, and the residual shear stress following spring-back are shown in Figure 9 assuming an erfc relaxation profile.

3.2 | Experimental procedure

A silica glass rod (GE 214) with radius $r_o = 3.515 \pm 0.010$ mm and a 10 cm long gage section was used for the shear stress relaxation experiment. GE 214 has a shear modulus, G, of

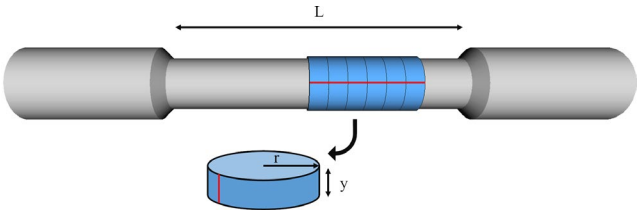

FIGURE 10 Schematic of shear relaxation sample geometry. Gage section was cut and polished to a consistent thickness for six samples. Dimensions indicated correspond to those in Equation 11 and Equation 12. The line across the section surface corresponds to the scribe mark used for section alignment [Color figure can be viewed at wileyonlinelibrary.com]

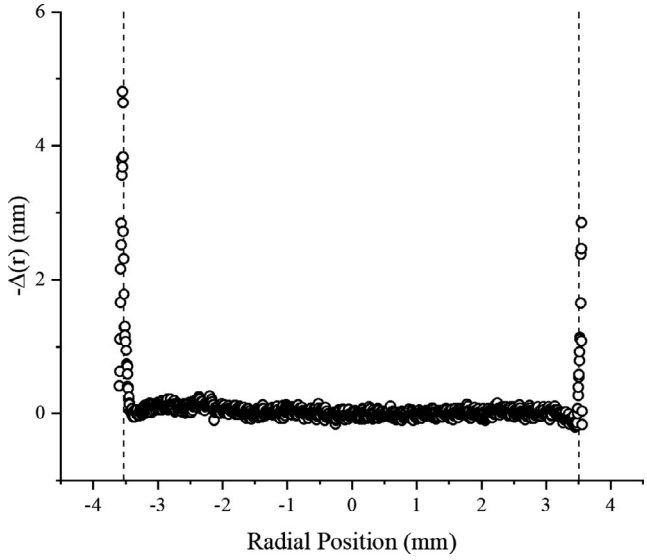

FIGURE 11 A superposition of six individual radial profiles is shown, confirming the predicted residual surface stress form but lacking necessary detail for fitting. The vertical lines mark the sample surface

31.6 GPa.[8] A shear strain was applied to the rod by applying a constant angle of twist, giving $T(0) = 0.6805\ N{\cdot}m$, $\frac{q}{L} = 0.08978\ rad{\cdot}m^{-1}$, and $\tau_{max} = 9.978$ MPa. The sample was heat-treated at 650°C for 4 days in air with 7 Torr (~ 1 KPa) of water vapor. The gage section of the rod was cut and sectioned according to Figure 10 and the circular faces of each cylinder were mechanically ground using silicon carbide paper from 400 to 1200 grit in water followed by a final chemical-mechanical polish using cerium oxide and water slurry. This procedure allowed retardance to be measured over a constant thickness. Six cylinders were cut and polished concurrently, resulting in a final thickness of 2.800 ± 0.014 mm. Rotational alignment was maintained by scribing a shallow scratch along the sample (see the red line in Figure 10).

Retardance in the glass cylinders was measured by passing polarized light through the sample along the y direction in Figure 10. Samples were immersed in index-matching fluid during measurement in order to mitigate scattering at the sample surface. The stress distribution is related to the retardance measurement by

$$\Delta(r) = C \cdot y \cdot \tau_{res} \tag{25}$$

where y is the thickness of the cylinder. The stress optic coefficient C can be shown to be the same value for shear and normal stresses in birefringent glasses.[23] In this work, C was estimated to be 3.0 Brewsters [$10^{-12} Pa^{-1}$] based on values measured for similar silica compositions.[13] The retardance profile is thus fit using the parameter z since y, q/L, and r_o are known. The relaxation depth, z, and diffusivity of surface stress relaxation, D_{SSR}, calculated from the retardance profile was compared to the values calculated from Equation 19 for an erfc relaxation profile and the values calculated from Ref. 8 for a step function relaxation profile assuming complete relaxation from the surface to the depth z and no relaxation elsewhere (see Equation 26).

$$T(t) = \frac{q \cdot G \cdot \pi}{2L} \left(r_0 - z\right)^4 \tag{26}$$

3.3 | Results

Retardance measurements were taken from six low-magnification images and averaged to generate a representative profile (see Figure 11). A higher magnification image

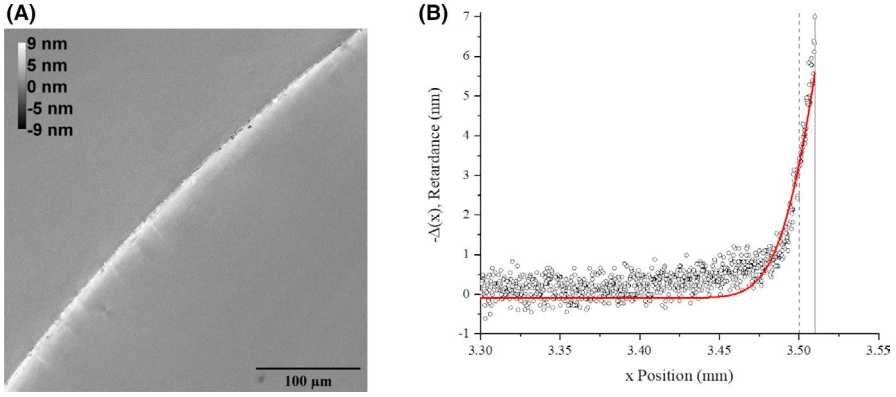

FIGURE 12 (A) High magnification image of the sample surface. The sample section interior is shown in the bottom right while the index-matching oil is in the upper left. (B) Radial profile fit to Equation 24. The relaxation depth z is indicated by the dashed line and the sample surface is indicated by the solid line [Color figure can be viewed at wileyonlinelibrary.com]

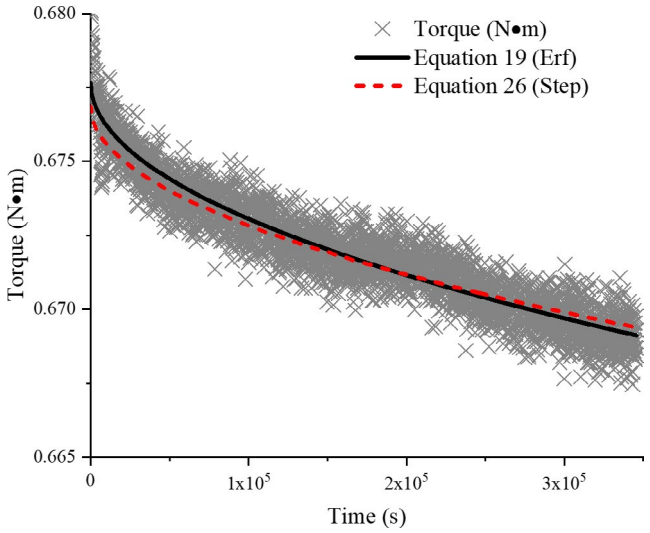

FIGURE 13 Torque relaxation during heat treatment fit using Equation 19 and Equation 26 [Color figure can be viewed at wileyonlinelibrary.com]

was taken in order to better resolve the surface retardance as shown in Figure 12. The depth of surface stress relaxation in Figure 12b was estimated by fitting Equation 24 and Equation 25 to the retardance profile. Rotation of sample did not alter the birefringence pattern, indicating a circular symmetry of the residual stress, as expected.

The torque relaxation depth was also estimated using Equation 19 and Equation 26, as shown in Figure 13.[8] The diffusion depth estimates from optical measurement and torque relaxation are given in Table 2 along with the diffusivity for surface stress relaxation from Equation 1. It was observed that the surface relaxation depth determined by optical retardance was greater than that determined by relaxation kinetics.

3.4 | Discussion

Application of the error function fit retains the consistency of the simpler step function for fitting the measured torque relaxation, while also allowing for fitting of the measured retardance profile. This compatibility further affirms that torque relaxation follows the developed surface stress relaxation model. Retardance measurement of the residual stress finds a diffusivity which is higher than the torque relaxation fit regardless of assumptions regarding relaxation profile. In order to confirm that the observed larger surface stress relaxation diffusion coefficient obtained by birefringence was not caused by sample thickness variation (i.e., non-uniform thickness near the sample surface), deviation from the sample thickness as measured using a micrometer was found as a function of radial position (see Figure 14). This deviation was obtained by use of a contact profilometer, which measured change in relative height from the sample surface up to one edge. The change in thickness (~0.035%) was found to be sufficiently small as to not significantly affect the retardance measurement. This thickness variation accounts for possible retardance variance of only ±0.024 nm.

The observed difference between torque relaxation and retardance-measured z values is likely due to a combination of the greater sensitivity of the retardance measurement as well as the surface roughness at the cylindrical face of the sample (a consequence of sample machining before heat treatment), leading to slightly deeper relaxation than predicted for a perfect cylinder. This machined surface is preferable however to a smooth flame-polished surface, as it has been shown that flame polishing introduces OH groups into the glass surface, thereby altering relaxation behavior.[24] Other possible sources of error are similar to that of the optical fiber experiment, such as changes in the stress optical coefficient or shear modulus of the glass following water diffusion.

TABLE 2 Comparison of surface shear stress relaxation depth and diffusivity by method

Method	Equation	z [μm]	D_{SSR} [cm^2/s]
Optical retardance	Equation 25	16.9	8.25×10^{-12}
Torque relaxation, erf relaxation profile	Equation 19	9.89	2.84×10^{-12}
Torque relaxation, step relaxation profile[8]	Equation 26	10.9	3.43×10^{-12}

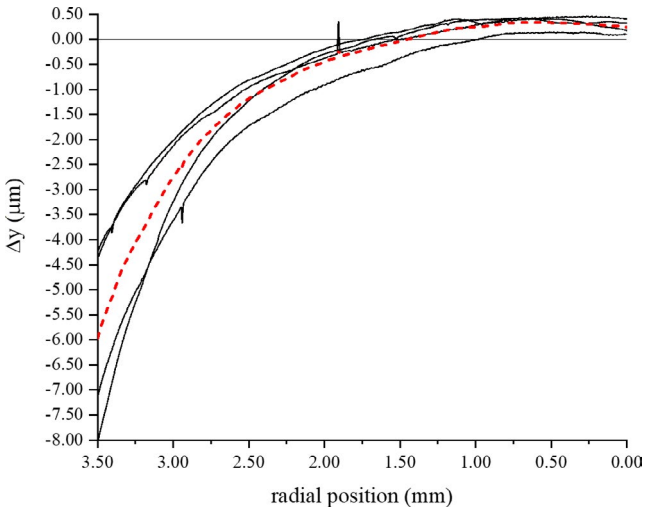

FIGURE 14 Deviation from thickness measured using a micrometer as a function of radial position for one sample, as measured using a profilometer. The solid curves are profiles measured from several sample rotations, with an average given by the dashed line. Maximum change in depth near the sample surface was found to be about 10 microns [Color figure can be viewed at wileyonlinelibrary.com]

4 | CONCLUSION

Low-temperature stress relaxation has been confirmed to occur in the near-surface region of bent silica fibers as well as in sheared silica rods using optical retardance measurements. The stress distribution as calculated from retardance measurements agrees with the expected result, assuming a diffusion-controlled relaxation using the complementary error function. Agreement with the model is good across a large time and temperature range in bending. Differences in low-temperature bending relaxation in the tensile and compressive surfaces, as indicated by the retardance measurements at 300°C agree with previous observations. In shear, torque relaxation measurements were found to agree well with the measured retardance profile, both of which can be modeled with good agreement to diffusion-based surface stress relaxation.

ACKNOWLEDGMENT

This research was supported by the NSF grant DMR-1713670 and Corning, Inc.

ORCID

Bronson D. Hausmann https://orcid.org/0000-0003-1448-3392
Emily M. Aaldenberg https://orcid.org/0000-0002-3137-9493

REFERENCES

1. Tomozawa M, Lezzi PJ, Hepburn RW, Blanchet TA, Cherniak DJ. Surface stress relaxation and resulting residual stress in glass fibers: A new mechanical strengthening mechanism of glasses. J Non-Cryst Solids. 2012;358:2650–62.
2. Lezzi PJ, Tomozawa M, Hepburn RW. Confirmation of thin surface residual compressive stress in silica glass fiber by FTIR reflection spectroscopy. J Non-Cryst Solids. 2014;390:13–8.
3. Lezzi PJ, Tomozawa M, Blanchet TA. Evaluation of residual curvature in two-point bent glass fibers. J Non-Cryst Solids. 2013;364:77–84.
4. Lezzi PJ, Tomozawa M. An overview of the strengthening of glass fibers by surface stress relaxation. Int J Appl Glass Sci. 2015;6(1):34–44.
5. Seaman JH, Lezzi PJ, Blanchet TA, Tomozawa M. Modeling slow crack growth behavior of glass strengthened by a subcritical tensile stress using surface stress relaxation. J Am Ceram Soc. 2015;98(10):3075–86.
6. Lezzi PJ, Seaman JH. Static fatigue and compressive stress generation in an aged crack. J Am Ceram Soc. 2018;101(4):1526–36.
7. Seaman JH, Blanchet TA, Tomozawa M. Origin of the static fatigue limit in oxide glasses. J Am Ceram Soc. 2016;99(11):3600–9.
8. Aaldenberg EM, Aaldenberg JS, Blanchet TA, Tomozawa M. Surface shear stress relaxation of silica glass. J Am Ceram Soc. 2019;102(8):4573–82.
9. Matthewson MJ, Kurkjian CR, Gulati ST. Strength measurement of optical fibers by bending. J Am Ceram Soc. 1986;69(11):815–21.
10. Chu PL, Whitbread T. Measurement of stresses in optical fiber and preform. Appl Opt. 1982;21(23):4241–5.
11. Park Y, Ahn T-J, Kim YH, Han W-T, Paek U-C, Kim DY. Measurement method for profiling the residual stress and the strain-optic coefficient of an optical fiber. Appl Opt. 2002;41(1):21–6.
12. Mori A, Tomita R. Semi-automated Sènarmont method for measurement of small retardation. Instrum Sci Technol. 2015;43(4):379–89.
13. Aben H, Guillemet C. Basic photoelasticity. Photoelasticity of Glass. New York: Springer; 1993:51–68.
14. Lezzi PJ, Seaman JH, Tomozawa M. Strengthening of E-glass fibers by surface stress relaxation. J Non-Cryst Solids. 2014;402:116–27.
15. Lagakos N, Mohr R, El-Bayoumi OH. Stress optic coefficient and stress profile in optical fibers. Appl Opt. 1981;20(13):2309.
16. Agarwal A, Davis KM, Tomozawa M. A simple IR spectroscopic method for determining fictive temperature of silica glasses. J Non-Cryst Solids. 1995;185:191–8.
17. Kuzuu N. Characteristic temperature, fictive temperature. In: Kawazoe H, editor. Pract. Handb. Amorph. Siliceous Mater. Tokyo: Realize Inc.; 1999:91–8.
18. Hausmann BD, Miller PA, Aaldenberg EM, Blanchet TA, Tomozawa M. Modeling birefringence in SiO_2 glass fiber using surface stress relaxation. J Am Ceram Soc. 2020;103(3):1666–76.
19. Aaldenberg EM. Fast stress relaxation at the surface of silica glass: Mechanism and effects. Troy, NY: Rensselaer Polytechnic Institute; 2019.
20. Agarwal A, Tomozawa M, Lanford WA. Effect of stress on water diffusion in silica glass at various temperatures. J Non-Cryst Solids. 1994;167:139–48.
21. Davis KM, Tomozawa M. Water diffusion into silica glass: Structural changes in silica glass and their effect on water solubility and diffusivity. J Non-Cryst Solids. 1995;185:203–20.
22. Tomozawa M, Davis KM, Seaman JH, Aaldenberg EM. The origin of anomalous water diffusion in silica glasses at low temperatures. J Am Ceram Soc. 2017;100(10):4548–61.
23. Onogi T, Inoue T, Osaki K. Shear birefringence measurement on amorphous polymers around the glass transition zone. J Soc Rheol Jpn. 1998;26(4):237–41.
24. Kim BH, Han SR, Paek U-C, Han W-T. Diffusion of OH in optical fiber preform by oxy-hydrogen burner. J Non-Cryst Solids. 2004;349:248–53.

How to cite this article: Hausmann BD, Aaldenberg EM, Tomozawa M. Photoelastic confirmation of surface stress relaxation in silica glasses: Fiber bending and rod torsion. *J Am Ceram Soc*. 2021;104:3087–3096. https://doi.org/10.1111/jace.17690